11 Particle physics with the CMS experiment at CERN

T. Årestad, L. Caminada, F. Canelli, V. Chiochia, A. de Cosa, C. Galloni, A. Hinzmann, T. Hreus, B. Kilminster, C. Lange, J. Ngadiuba, D. Pinna, P. Robmann, D. Salerno, S. Taroni, M. Verzetti, and Y. Yang

in collaboration with the:

CMS - Collaboration

After the recent discovery at the LHC of a Higgs-like particle [1, 2], studying its properties is among the primary goals and challenges of the next LHC run. Another goal are searches for new particles with masses around a TeV that could be produced directly at the LHC, after its upgrade.

Cosmological and astronomical observations have uncovered the existence of dark matter (DM). If DM is indeed a stable neutral weakly interacting particle with mass less than around a TeV as expected, we must produce it at the LHC so the LHC may well bridge the gap between the shortest and the largest distance scales.

The LHC delivered proton collisions until February 2013 concluding the first three-year running period (Run 1) in which CMS collected an integrated luminosity of 23.3 (6.1) fb^{-1} at the centre-of-mass energy $\sqrt{s} = 8$ (7) TeV. The next data-taking period (Run 2) at a higher center-of-mass energy of 13 TeV should have started by the time this report came to print.

[1] CMS collaboration, Phys. Lett. B **716** (2012) 30.
[2] ATLAS collaboration, Phys. Lett. B **716** (2012) 29.

11.1 The CMS detector

CMS [1, 2] is a multipurpose detector designed for a variety of particle physics studies at the LHC. CMS consists of different detector layers (see Fig. 11.1). An all-silicon tracker, an electromagnetic calorimeter, and a hadronic sampling calorimeter are all contained within a large-bore 3.8 T superconducting solenoid. Beyond the solenoid are four layers of muon detectors. The CMS

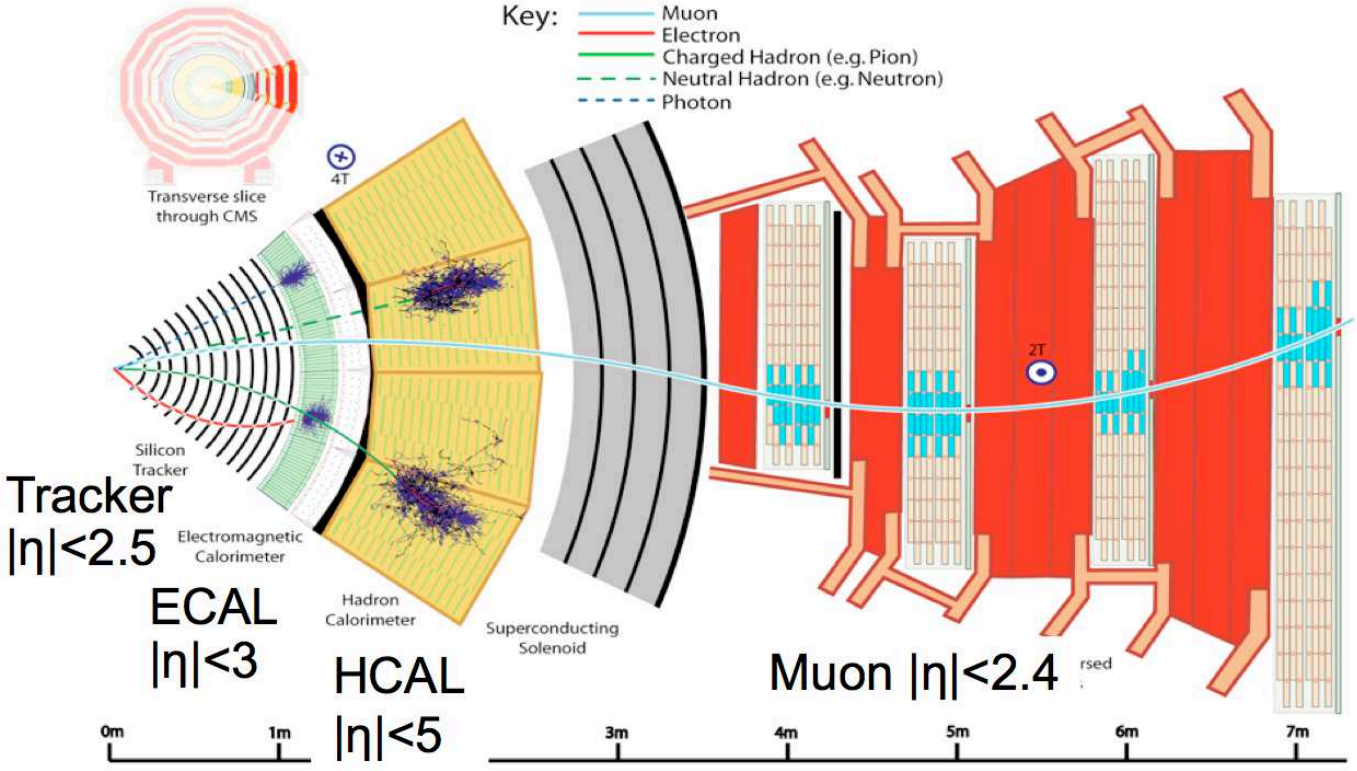

FIG. 11.1 – Schematic view of a sector of the CMS detector, illustrating how muons, electrons, charged hadrons, neutral hadrons and photons are reconstructed.

tracker is composed of the inner pixel detector and the outer silicon strip detector. The pixel detector consists of three barrel layers (BPIX) at 4.4, 7.3, and 10.2 cm, and two forward/backward disks (FPIX) at longitudinal positions of $\pm$34.5 cm and $\pm$46.5 cm and extending in radius from about 6 to 15 cm. BPIX was built by the CMS Swiss Consortium: PSI, ETH and the University of Zurich.

The high segmentation of the pixel detector permits the building of seed clusters for the tracking algorithm reconstruction and also for the fast online track reconstruction in the high level trigger (HLT). The pixel detector is used for electron/photon identification and muon reconstruction, and its high resolution is crucial for accurate vertex reconstruction, which also allows the identification of long-lived τ-leptons and B-hadrons traveling a few millimeters before decaying.

Members of our group cover important coordination roles within the CMS collaboration. A. de Cosa is the level3 pixel monitor coordinator, C. Lange acts as convener of the CMS pixel data acquisition group, L. Caminada coordinates the supply tube subgroup within the CMS pixel phase 1 upgrade project and serves as ex-officio member of the Tracker conference committee, A. Hinzmann is former co-convener of the Exotica in jet final states physics group and current convener of the the JetMET algorithms and reconstruction group, Y. Yang serves as the CMS Monte Carlo request manager, B. Kilminster is co-convener of the phase 2 upgrade future Higgs physics group, F. Canelli is co-convener of the Beyond 2 Generations Very Heavy Fermions subgroup, T. Hreus coordinates the Tracker Detector Performance Group, in charge of the tracker offline software and operations, while V. Chiochia is a member of the CMS conference committee and B-physics steering group. In addition, L. Caminada (taking over from S. Taroni) and C. Lange are members of the Swiss CMS Tier3 steering committee. Currently F. Canelli holds the position of group leader.

[1] CMS collaboration, CERN-LHCC 2006-001.

[2] CMS collaboration, JINST **3** (2008) S08004.

In what follows, we describe the contributions of our group, which were focused in three main areas of research: physics measurements and searches, analysis techniques that benefit these physics analyses, and the operation and upgrade of one of the detectors vital to these measurements. A primary physics focus was on the better understanding of the Higgs sector. We also searched for new particles motivated by DM, SUSY, and extra dimensions, which could be in reach of LHC energies and luminosities.

11.2 Higgs boson couplings to top quark pairs

The Higgs boson was first observed through its decay into ZZ and $\gamma\gamma$. Also in the decay channel to WW a significant signal could be established. Furthermore, evidence for Higgs couplings to up-type fermions was found at the Tevatron in the decay $H \to b\bar{b}$ [1], and, more recently, in $H \to b\bar{b}$ and $H \to \tau\tau$ at the LHC [2–5] where our group contributed significantly, as documented in last year's annual report. Since the properties of Higgs bosons belonging to extended Higgs sectors differ from SM predictions, accurate measurements of Higgs couplings are important to identify possible deviations that indicate new physics scenarios.

Evidence of a direct coupling to up-type fermions, in particular to top quarks, is still lacking. Since the top quark is the heaviest particle of the SM, the only way to directly probe such coupling is by studying the associated production of a Higgs boson and a pair of top quarks ($t\bar{t}H$). This channel is challenging, given the small cross section and high QCD background. The $H \to b\bar{b}$ decay is most promising thanks to the large branching ratio and the high efficiency of tagging jets from b-quark hadronization. Nevertheless, the QCD background $pp \to t\bar{t} + b\bar{b}$ remains irreducible with respect to b-tagging, and dominates the signal by far [6].

We are leading a search for $t\bar{t}H$ based on the analytical Matrix Element Method (MEM) [7] for optimal separation of $t\bar{t}H$ signal and $pp \to t\bar{t} + b\bar{b}$ background. We use the 8 TeV data from 2012, corresponding to an integrated luminosity of 19.0 fb^{-1} [8]. Events are selected, in which at least one top quark decays leptonically through $t \to bW$, with $W \to \ell\nu_\ell$, $\ell = e, \mu$, and the other W decay may proceed hadronically ($W \to q'\bar{q}$). Event classes are defined according to lepton and jet multiplicities to take advantage of the different signal to background ratios. Single-lepton (SL) and double-lepton (DL) events contain exactly one lepton or an opposite-sign lepton pair, respectively. The b-tagger discriminator of jets is based on secondary vertex information. For each event, a b-tag likelihood ratio is calculated, which optimally separates the hypotheses that either exactly four or two jets originate from b-quarks. Signal events as well as those from the irreducible $t\bar{t} + b\bar{b}$ background contain four b-quarks and thus have values of b_{LR} close to 1.0. Backgrounds containing light quarks tend to have values closer to zero.

The ratio of probability densities under the two competing hypotheses $t\bar{t}H$ and $t\bar{t} + b\bar{b}$ together with the b-tagging information is used to constrain the *signal strength modifier* $\mu \equiv \sigma/\sigma_{\mathrm{SM}}$, shown in Fig. 11.2. No evidence of a signal is found. The 95% CL upper limit under background-only hypothesis is $\mu < 3.3$. The observed limit, $\mu < 4.2$, corresponding to a best-fit value of

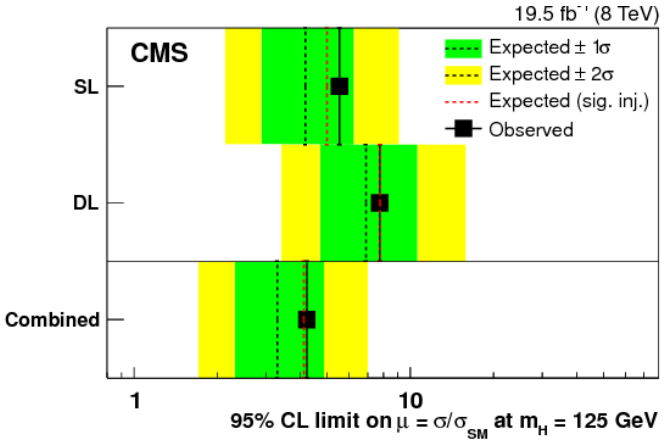

FIG. 11.2 – The 95% CL upper limit on μ, the $t\bar{t}H$ rate normalized to the SM prediction. Observed values are compared to the median expected limits under the background-only and the signal-plus-background hypotheses, both for the individual channels (see text) and their combination.

$\mu = 1.2^{+1.6}_{-1.5}$ represents an improvement by more than 20% over the result published previously.

Our focus now turns towards the higher energy data at 13 TeV becoming available in the coming months. We plan to include the all-hadronic decay channels of the top-quark pair, with a branching ratio as large as 46%, giving a significant increase in statistical accuracy.

[1] CDF and D0 collaborations, Phys. Rev. Lett. **109** (2012) 071804.

[2] CMS collaboration, JHEP **05** (2014) 104.

[3] ATLAS collaboration, JHEP **04** (2015) 117.

[4] CMS collaboration, Phys. Rev. D**89** (2014) 012003.

[5] ATLAS collaboration, JHEP **01** (2015) 069.

[6] A. Bredstein, Phys. Rev. Lett. **103**, (2009) 012002.

[7] D0 collaboration, Nature 429, 638-642 (2004); Phys. Lett. B **617** (2005) 23; M.F. Canelli, FERMILAB-THESIS-2003-22; CDF collaboration, Phys. Rev. Lett. **101** 252001 (2008); Phys. Rev. Lett. **103** 092002 (2009); Phys. Rev. Lett. **105** 042002 (2010); Phys. Rev. Lett. **99** 182002 (2007); Phys. Rev. D **84** 071105(R) (2011); Phys. Rev. Lett. **103** 101802 (2009); Phys. Rev. D **85** 072001 (2012).

[8] CMS collaboration, arXiv:1502.02485.

11.3 MSSM Higgs boson search

The low mass of the SM Higgs boson demands a mechanism for its stabilization, since naively radiative corrections should make it many orders of magnitude higher. SUSY, for instance, provides loop corrections to the Higgs mass that cancel divergent loops from known SM particles. Within the MSSM (Minimal Supersymmetric Model), there are four additional, heavier, Higgs bosons (two oppositely-charged scalars, one neutral scalar, and a neutral pseudoscalar) which could be in reach of the LHC since the favored masses are just above current limits. We are searching for neutral Higgs bosons decaying to $b\bar{b}$ within the MSSM framework, in association with a b-jet. The cross section is enhanced compared to SM value by a factor of $\tan^2(\beta)$, which could be as large as 1000. For $\tan^2(\beta) \geq 3$ the decay to $b\bar{b}$ has a branching ratio of about 90%.

A previous search at 7 TeV set lower limits on the MSSM Higgs mass up to 350 GeV [1], the most stringent bounds on MSSM Higgs-production in this final state. At 8 TeV $H \rightarrow b\bar{b}$ becomes more boosted and the fraction of events in which two B-hadron jets merge is significant. We found that the sensitivity improves by a special evaluation of such events. We have investigated variables (secondary vertex variables such as vertex mass) discriminating between single-b and two-b jets. Online b-tagging based on impact-parameter significance can cope with the large hadronic interaction rate at the LHC. Different mass ranges have been defined, for which we have optimized the event trigger. We also evaluated the non-QCD-multijet background events, and estimated the associated systematic uncertainties. With the help of recent higher-order MC event generator programs for the MSSM $b\bar{b}H$ process [2], we found that the acceptance differences between the leading and next-to-leading order predictions are small, which is of interest for all related MSSM Higgs analyses.

The new discriminant, called event b-tag, gives a handle on the background composition. The background consists largely of QCD multijet events which can be studied in the measured double-b-tag events. Our group performed exhaustive MC studies confirming the validity of this approach. A full 2D maximum likelihood fit to the invariant mass of the leading two b-jets and the event b-tag fixes the event yields, where a signal would show up as a bump. Results from the full 2012 dataset at 8 TeV will soon be published. We will extend the mass range of this search using the upcoming 13 TeV data.

[1] CMS collaboration, Phys. Lett. B **722**, 207 (2013).

[2] M. Wiesemann *et al.*, JHEP02,**2015**,132.

11.4 Search for $H \to e\tau$

The effective couplings of the Higgs particle with the SM fermions and gauge bosons are still poorly known. If the scalar sector of the theory is different from the SM expectation (e.g. in presence of more scalars), sizable deviations might occur. In particular, the suppressed couplings of the massive Higgs field to the light SM fermions do not need to be proportional to their masses and do not need to be flavor diagonal. Upper limits on such possible flavor-changing couplings have been derived from the precise low-energy constraints on FCNC processes, both in the quark and in the lepton sector [1, 2], before any attempt to directly access them in Higgs decay. Flavor-changing couplings in the quark sector, and the $h \to \bar{\mu}e, \bar{e}\mu$ couplings appear severely constrained already. Indirect constraints for couplings involving the τ lepton are, however, quite weak and $\mathcal{B}(h \to \tau\bar{\mu} + \bar{\mu}\tau)$ and $\mathcal{B}(h \to \tau\bar{e} + \bar{e}\tau)$ could be as large as 10%, well within reach of the LHC.

We have recently performed a direct search for $H \to \mu\tau$, resulting in a 2.5σ excess over the background expectation [3]. This result generated a great interest in the physics community and triggered the interest in other final states, such as the $e\tau$, discussed here.

The search was performed in the 19.7 fb^{-1} data sample at 8 TeV, looking at both $\tau \to \mu\nu_\mu\nu_\tau$ and $\tau \to \nu_\tau$+hadrons. We coordinate the analysis of the hadronic channel. Candidate events for Higgs production are grouped according to the number of jets: no jet gluon-gluon fusion (GGF), one jet boosted production, and two jets vector boson fusion (VBF). The main backgrounds are W + jets events, when a jet is misidentified as electron or τ, and Drell-Yan. Minor backgrounds involve $t\bar{t}$, single top and di-boson (WW, ZW and ZZ) production and $H \to \tau\tau$.

Both channels use the collinear mass, $M_{coll} = M_{vis}/\sqrt{x_{vis}}$ where M_{vis} is the mass reconstructed using only the visible decay products and x_{vis} is the fraction of τ momentum carried by the visible decay products. Events are selected requiring an electron with $p_T > 45$ (35, 35) GeV and τ_{had} candidates with $p_T > 30$ (40, 30) GeV for the 0 (1, 2) jet category. The electron and the τ are required to have opposite charge. A veto on the presence of additional leptons and jets is applied. No jets tagged as b-jets are allowed to reduce the $t\bar{t}$ and single top backgrounds. The additional requirements on the transverse mass of τ to the missing transverse energy (τ MET M_T), $M_T < 70$ (40, 50) GeV for the 0 (1, 2) jet category and, on the $\Delta\Phi$ of the $e - \tau$ pair for the 0-jet category, are applied to better discriminate the signal from W + jets and Drell-Yan backgrounds.

The collinear mass for the GGF category is shown in Fig. 11.3, where the data in the signal region are kept blind. The measured distribution in the mass sidebands is consistent with the sum of all backgrounds. Expected and observed limits are calculated in the CLs approach for a Higgs boson mass of 126 GeV. The expected upper limit on the branching ratio is found to be $(1.69 \pm 0.85)\%$ for the $H \to e\tau_{had}$. Combining both τ_{had} and τ_μ channels the expected upper limit is $(0.74 \pm 0.38)\%$. The study is currently in the final review phase and will be submitted for publication soon.

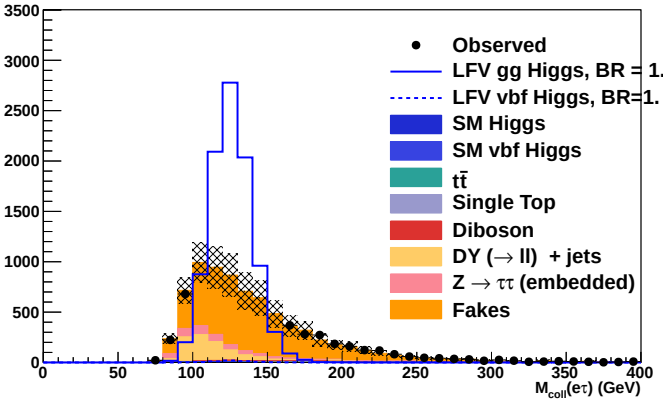

FIG. 11.3 – Collinear mass of the $e\tau_{had}$ final state (see text) in the zero-jet category after applying all the selection cuts. The measured distribution (still blinded in the signal region) is compared with the expected background contributions. The LFV Higgs signal is enhanced for better visualization.

[1] G. Blankenburg, J. Ellis and G. Isidori, Phys. Lett. B **712** (2012) 386.

[2] R. Harnik, J. Kopp and J. Zupan, JHEP **1303** (2013) 026.

[3] CMS collaboration, CMS-PAS-HIG-14-005.

11.5 Search for dark matter particles with top quarks

In several BSM models, like SUSY, a weakly interacting massive particle (WIMP) arises naturally as a DM candidate. So far, however, there is no established knowledge about its properties, including its mass and interactions with ordinary matter [1, 4].

The interaction Lagrangian between DM particles and quarks can be described by an effective field theory (EFT) with an interaction scale M_*, where the form of the Lagrangian depends on the type of the interaction. For scalar interaction, the coupling strength scales with the quark mass,

$$\mathrm{L_{int}} = \frac{m_q}{M_*^3}\bar{q}q\bar{\chi}\chi$$

so couplings to light quarks are suppressed and traditional inclusive mono-jet searches are not very sensitive [4–11].

In our analysis, we look for DM produced in association with a top-quark pair. The search is performed in the dilepton [12] and single-lepton channel [13], with large

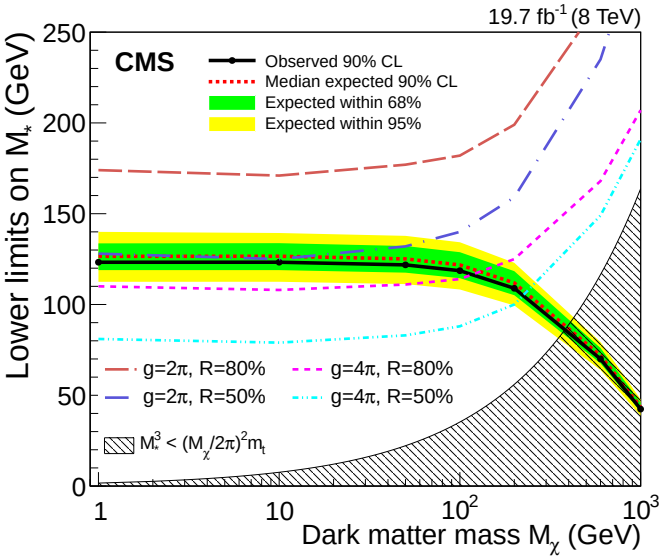

FIG. 11.4 – Observed 90% CL exclusion limits in the plane of DM particle mass and interaction scale. The background-only expectation and the 68% and 95% CL bands are indicated. A lower bound of the validity of the EFT is indicated by the upper edge of the hatched area. The four curves represent the lower bound on M_* for which 50% and 80% of signal events have a pair of DM particles with an invariant mass less than $g\sqrt{M_*^3/m_t}$.

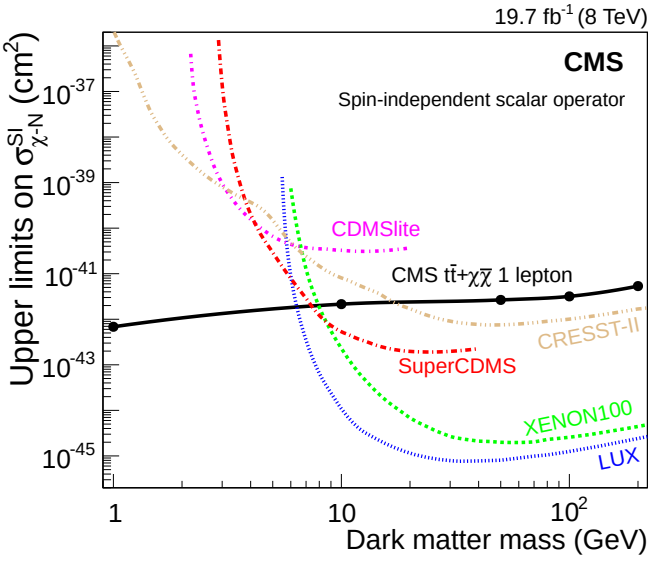

FIG. 11.5 – The 90% CL upper limits on the DM-nucleon spin-independent scattering cross section ($\sigma^{\mathrm{SI}}_{\chi\text{-N}}$) as a function of the DM particle mass for the scalar operator considered here. Also shown are 90% CL limits from various direct DM search experiments.

transverse missing energy ($E_{\mathrm{T}}^{\mathrm{miss}}$). The single-lepton channel, which is particularly sensitive, shows no signal above SM background, excluding cross sections larger than 22 to 55 fb (90% CL) for DM particles with mass between 1 GeV and 1 TeV. These results translate into new lower limits on M_*, as shown in Fig. 11.4.

In preparation of DM searches for Run 2 the analysis has been extended to the fully hadronic channel. The sensitivity is comparable to the single-lepton channel.

In addition to top quarks, DM can also be produced in association with bottom quark pairs, providing a striking signature. DM signals are characterized by large $E_{\mathrm{T}}^{\mathrm{miss}}$, one or two b-tagged jets and no other significant activities in the detector. The channel is expected to have sensitivity similar to the previous one.

The limits on the interaction scale M_* have been translated into limits on the DM-nucleon scattering cross section for the scalar operator considered here (see Fig. 11.5): 90% CL upper limits are a few times $10^{-42}\mathrm{cm}^2$ and represent the most stringent limits below 6 GeV.

[1] Planck collaboration, arXiv:astro-ph/1303.5076.

[2] V. Trimble, Ann. Rev. Astrophys., **25** (1987) 425.

[3] E. Komatsu *et al.*, Astrophys. J. Suppl., **192** (2011) 18.

[4] J. L. Feng, Ann. Rev. Astron. Astrophys., **48** (2010) 495.

[5] J.M. Beltran *et al.*, JHEP **17** (2010) 1.

[6] J. Goodman *et al.*, Phys. Lett. B **695** (2011) 185; Phys. Rev. D, **82** (2010) 116010.

[7] P. J. Fox *et al.*, Phys. Rev. D **85** (2012) 056011; Phys. Rev. D **86** (2102) 015010.

[8] Rajaraman *et al.*, Phys. Rev. D **84** (2011) 095013.

[9] T. Lin, E.W. Kolb, and L.-T. Wang, Phys. Rev. D **88** (2013) 063510.

[10] CMS collaboration, Tech. Rep. CMS-PAS-EXO-12-048, 2012.

[11] ATLAS collaboration, JHEP, **1304**, 2013; Tech. Rep. ATLAS-CONF-2012-147, CERN, Nov 2012.

[12] CMS collaboration, CMS-PAS-B2G-13-004.

[13] CMS collaboration, arXiv:1504.03198.

11.6 Dijet angular distributions and search for new physics

High momentum-transfer proton-proton collisions at the CERN LHC probe the dynamics of the underlying interaction at distances below 10^{-19} m. Often these collisions produce a pair of jets (dijets) approximately balanced in transverse momentum. These dijet events provide an ideal testing ground to probe the validity of perturbative QCD and to search for new phenomena such as quark compositeness or additional, compactified spatial dimensions. A particularly suitable observable for this purpose is the dijet angular distribution expressed in terms of $\chi_{\mathrm{dijet}} = \exp(|y_1 - y_2|)$, where y_1 and y_2 are the rapidities

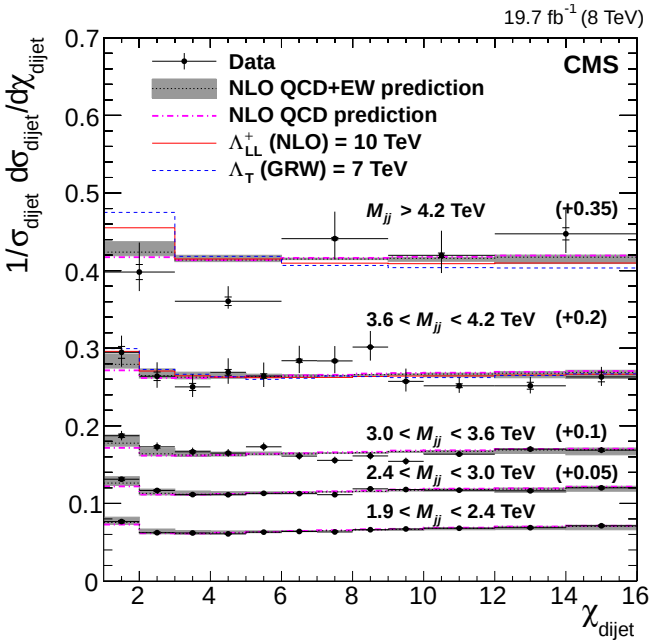

FIG. 11.6 – Normalized χ_{dijet} data distributions corrected for detector effects are compared to NLO predictions with electroweak corrections and no significant deviation is found. The predictions for a signal from quark compositeness Λ^{+}_{LL} and extra dimensions Λ_T are overlaid.

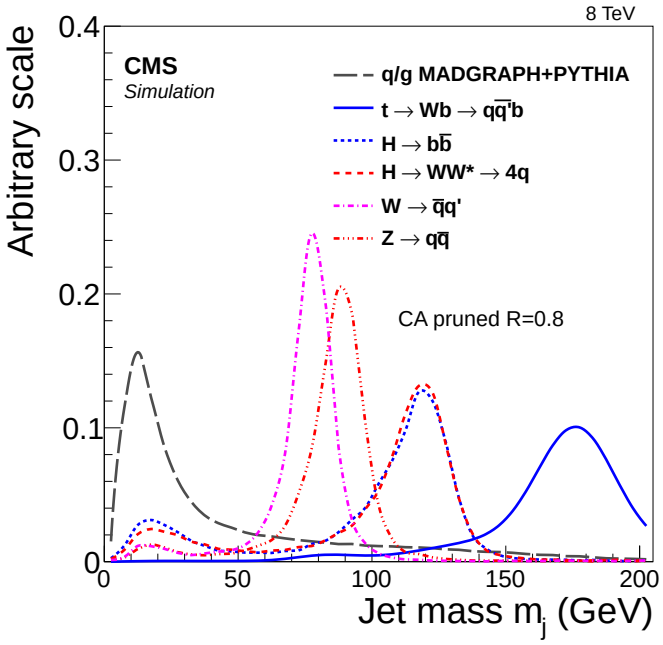

FIG. 11.7 – Distribution of pruned jet mass in simulation of signal and background processes.

of the two jets with the highest transverse momenta. In perturbative QCD the dijet angular distribution at small c.m. scattering angles is approximately independent of the underlying partonic level process and exhibits behavior similar to Rutherford scattering, characteristic of spin-1 particle exchange. Signatures of new physics, such as quark compositeness visible to us as quark contact interactions or virtual exchange of Kaluza–Klein excitations of the graviton in extra dimension models, that exhibit angular distributions that are more isotropic than those predicted by QCD, could appear as an excess of events at low values of χ_{dijet}.

We performed a search based on a data set corresponding to an integrated luminosity of 19.7 fb^{-1} [1]. Dijet angular distributions unfolded for detector effects are found to be in agreement with the perturbative QCD predictions that include electroweak corrections (see Fig. 11.6). Limits on the contact interaction scale from a variety of models at next-to-leading order in QCD corrections are obtained. A benchmark model in which only left-handed quarks participate is excluded up to a scale of 9.0 (11.7) TeV for destructive (constructive) interference at 95% CL. Lower limits between 5.9 and 8.4 TeV on the scale of virtual graviton exchange are extracted for the Arkani-Hamed–Dimopoulos–Dvali model of extra spatial dimensions.

[1] CMS collaboration, arXiv:1411.2646.

11.7 Search for heavy resonances in diboson events

The SM does not explain why the strengths of the electroweak force and gravity differ by 36 orders of magnitude. Composite Higgs models and models of large extra dimensions [1, 2], which do provide a natural solution to this hierarchy problem, predict many new particles such as additional W' and Z' gauge bosons. These bosons can have large branching ratios for decays into W, Z and H bosons, while the decay to fermions is suppressed.

We have searched for such new heavy particles decaying to pairs of bosons in the 2012 data. The recently proposed Heavy Vector Triplet (HVT) model [3] generalizes a large class of explicit models predicting new heavy spin-1 vector bosons and we use it to interpret our search results in a more general framework.

11.7.1 Exploiting jet substructure

The final states described above are accessible through novel jet substructure techniques identifying the bosons by what is called W/Z- or Higgs-tagging. The bosons decay predominantly into quarks which transform into sprays of particles (jets). Unfortunately, for heavy resonances reachable at the LHC, the bosons have such high momenta that their decay products merge into a single jet. In order to distinguish the substructure of these jets we have demonstrated and tested a variety of W/Z-tagging algorithms. The best scheme is based on the Lorentz invariant jet mass with the so-called pruning algorithm [4] and the jet shape variable N-subjettiness [5], which is an

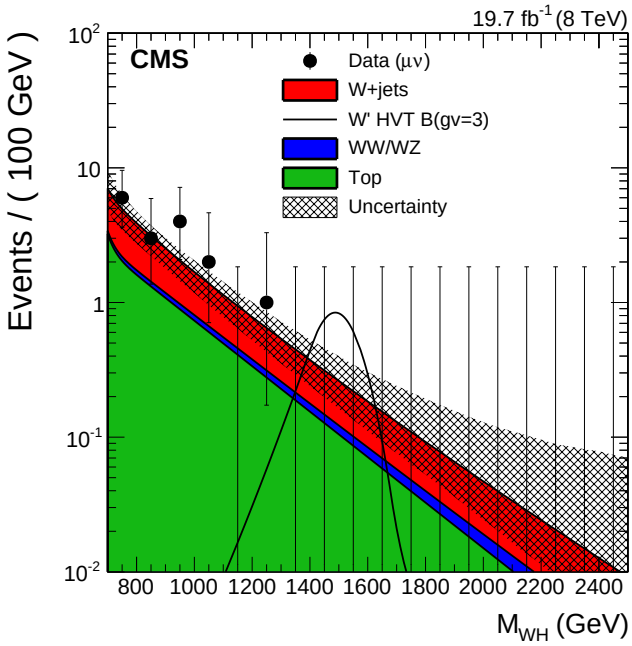

FIG. 11.8 – Distribution of m_{WH} for data and expected backgrounds for the muon category. Also shown is a hypothetical W' signal with mass of 1500 GeV.

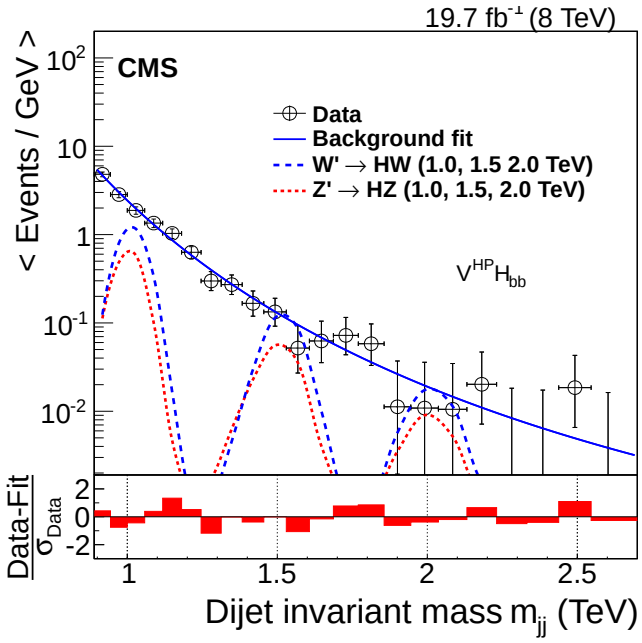

FIG. 11.9 – The final dijet mass distribution fit for a signal-like resonance. No signal is observed, and upper limits on the cross-section are set.

indicator for the number of hard quarks in the jet. The pruning algorithm separates the particles from quarks originating in boson decay from those consistent with background-like QCD radiation are filtered out (see Fig. 11.7). Our technique has been employed in the most recent CMS searches.

11.7.2 Search for new heavy bosons with b-tagged jets and tau leptons in the boosted regime

We investigated the decay of a charged heavy vector boson W' into a W and a Higgs boson, which is one of the first studies of an exotic final state with a Higgs boson. For a W' mass between 1 and 3 TeV, the resulting energetic decay products tend to be very collimated. The selected signature, a leptonic W decay in combination with a Higgs decaying into two b-quarks, is characterized by an isolated high p_T lepton, large missing transverse energy and two high p_T jets which are expected to be highly collimated into a single jet. The jet pruning and N-subjettiness algorithms mentioned above have been implemented and the presence of b-quarks is exploited. Additional challenges emerge when the secondary vertices from the B hadrons overlap. As illustrated in Fig. 11.8, no signal was observed and a strongly coupled vector resonance with mass below 1.5 TeV has been excluded [6]. Using the same techniques for W/Z/H identification, our group also performed a search for heavy resonances, denoted as X, in the process $X \to ZH \to q\bar{q}b\bar{b}$ and $X \to WH \to q\bar{q}'b\bar{b}$, looking for a bump on a smoothly falling background as shown in Fig. 11.9. This search yields the current most stringent limits in this final state on a strongly coupled vector resonance with mass up to 1.7 TeV [7].

We also search for heavy resonances, in the process $X \to ZH \to qq\tau\tau$ and $X \to HH \to b\bar{b}\tau\tau$. The fact that the τ leptons decay products may overlap makes the τ reconstruction challenging. The hadronic τ identification is performed by algorithms based on jet reconstruction with particle-flow techniques [9]. Since this might fail for overlapping energy deposits we have developed special reconstruction techniques. We remove from consideration energy deposits from each subdetector associated with each identified τ, and recalculate the isolation.

No BSM signals were found in the $Z + H$ final state [8]. From a combination of all possible decay modes of the τ leptons, production cross sections in a range between 0.9 and 27.8 fb are excluded at 95% CL, depending on the resonance mass. The $X \to HH \to b\bar{b}\tau\tau$ is currently nearing completion and will have similar sensitivity.

11.7.3 Preparation studies for Run II

The increased beam intensities and energies in Run 2 adversely affect the performance of substructure quantities for V tagging. Typically 30 to 40 proton-proton collisions will accompany an event of interest giving pileup. Moreover, the increase in center-of-mass collision energy from 8 TeV to 13 TeV will raise the production rate and energies

of highly boosted objects challenging the jet reconstruction algorithms and degrading the discriminating power of V tagging variables. Such degradation was observed for jet momenta above 1.5 TeV with the algorithms used in Run 1, due to breakdowns in particle reconstruction techniques [10].

The CMS ECAL granularity is five times finer than HCAL in both η and ϕ, which improves the ability to detect high-p_{T} jet substructure. We studied different scenarios with different treatment of reconstructing neutral particles from ECAL and HCAL energy left after charged hadron reconstruction [11] and we are able to maintain the current V tagging performance up to $p_{\mathrm{T}} = 3.5$ TeV at an average of 40 pileup interactions. It follows that CMS will effectively provide substructure observables across the full range of jet p_{T} expected in Run 2.

The di-boson resonance searches our group has performed during Run 1 are a very useful preparation for Run 2 when the sensitivity to new physics signals will overtake the Run 1 results within a couple of months. We are prepared for the search for high mass diboson resonances setting up the full analysis work-flows to be run immediately once the data comes in.

[1] L. Randall and R. Sundrum, Phys. Rev. Lett. **83** (1999) 3370.

[2] K. Agashe, H. Davoudiasl, G. Perez *et al.*, Phys. Rev. D **76** (2007) 036006.

[3] D. Pappadopulo *et al.*, arXiv:1402.4431.

[4] S.D. Ellis, C.K. Vermilion, and J.R. Walsh, Phys.Rev. D **81** (2010) 094023.

[5] J. Thaler and K. Van Tilburg, JHEP **1103** (2011) 015.

[6] CMS collaboration, CMS-PAS-EXO-14-010.

[7] CMS collaboration, CMS-PAS-EXO-14-009.

[8] CMS collaboration, CMS-PAS-EXO-13-007.

[9] CMS collaboration, CMS-PAS-PFT-09-001 (2009).

[10] CMS collaboration, JHEP **12** (2014) 017.

[11] CMS collaboration, CMS-PAS-JME-14-002.

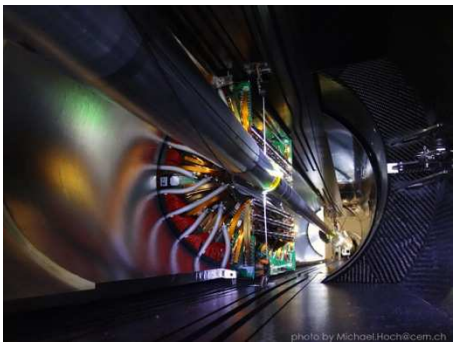

FIG. 11.10 – One half of the barrel pixel detector after re-installation in CMS.

11.8 Detector maintenance, operations, and upgrades

Our group is dedicated to operating, maintaining, and upgrading the barrel pixel detector (BPIX), which our institute helped to build. The detector allows for high precision tracking and to reconstruct secondary vertices from heavy quark or τ-lepton decays and is a key element for most analyses in our research portfolio. Its location closest to the interaction point results in a high track multiplicity and heavy irradiation.

11.8.1 Pixel detector maintenance and operation

The pixel detector, installed in 2008, showed excellent performance during the first LHC run with more than 97.7% of the channels working. After Run 1 finished in 2012, the detector was stored at low temperature in a dedicated clean room, equipped with all infrastructure needed to control and readout the detector. Faulty modules and optical components were replaced and preparations were made for Run 2.

In the course of its operation, the pixel detector suffered radiation damage, resulting in an increase of leakage current and bias voltage, charge trapping and signal degradation. We determined the optimal settings for the irradiated detector and tested the full detector at 0°C. Some sectors were also tested at −15°C as foreseen in Run 2 to mitigate radiation effects.

We took part in the reinstallation (see Fig. 11.10) and were responsible for the commissioning and calibration. A picture of the team, formed by our group and colleagues from PSI, INFN Padova and Hamburg University, is shown in Fig. 11.11. The installation of the BPIX was completed within a week, allowing to quickly proceed with the installation of the FPIX detector and the subsequent closure of CMS.

FIG. 11.11 – Pixel installation team after the successful completion of its task.

Furthermore, we are improving the software used to calibrate, monitor, record data, and reconstruct hits. During the long shutdown of the LHC, we migrated the software to the new infrastructure at the experimental site, and continuously improved its components. Changes in the CMS trigger and timing system made a new control software necessary ensuring the synchronization with the other CMS subdetectors.

11.8.2 Detector studies and improvements to the hit reconstruction

During the year 2012 the BPIX hit resolution in the transverse plane changed gradually from 8 μm to 9 μm (see Fig. 11.12). This degradation is attributed to changes in the detector conditions, such as alignment, gain calibration, Lorentz angle and irradiation. The pixel hit resolution is measured using the so called pixel triplet method [1] in which the actual hit position is compared with the value predicted by the two neighboring layers. This way we are also able to measure the hit efficiency for different detector conditions and irradiation scenarios and their impact on the hit resolution. So far we found no explanation for the degradation but studies are ongoing.

Our group has also worked on improving the reconstruction of pixel hits in collimated particle jets. When two charged particles traverse the sensors in close proximity, the pixel hits may overlap and merge into one larger cluster. The resulting merged hit is displaced with respect to the correct position and can lead to deterioration of tracking resolution and efficiency. More details are given in last year's report.

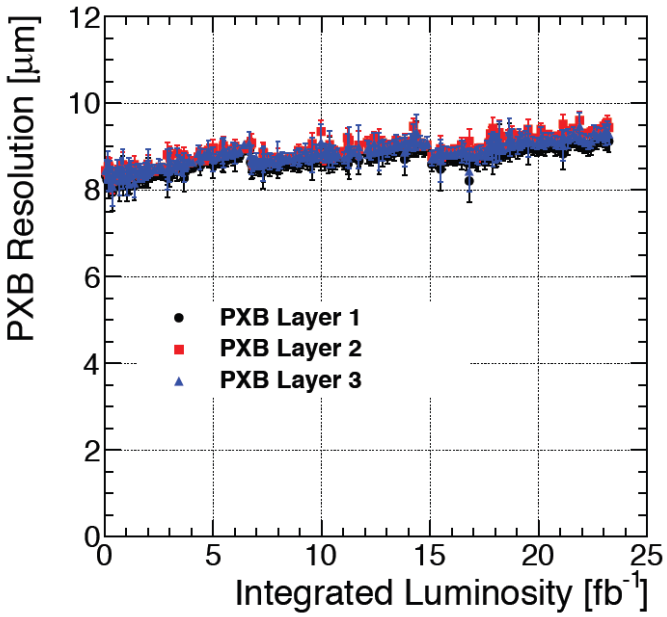

FIG. 11.12 – Hit resolution of the BPIX detector in the transverse plane ($r\phi$) as a function of the delivered integrated luminosity in the year 2012 [1].

11.8.3 Barrel pixel detector phase I upgrade

The current BPIX detector consists of three 57 cm long layers of silicon pixel modules serviced by 2.2 m of supply tubes which transport cooling tubes, electrical power, and optical signals. The University of Zurich designed, built and tested the mechanical support structure and the supply tubes, including the mechanical structure, cooling and service lines, and boards to transfer optical signals. For the BPIX phase 1 upgrade [2] we are again in charge of these components. The upgrade combines a new pixel readout chip with several other improvements to keep up performance during Run 2: The current 3-layer central pixel barrel, 2-disk forward pixel detectors are to be replaced with 4-layer central pixel barrel, 3-disk forward pixel detectors (Fig. 11.13) which makes a complete redesign of the detector and supply tube mechanics necessary. In order to reduce the amount of dead material which has a negative impact on the detector performance a new, light-weight cooling system will be installed. The new cooling system uses two-phase CO_2 cooling instead of single-phase C_6F_{14} liquid cooling. The tubes are much narrower, operate at 60 times higher pressure and show a complicated looping structure.

We have now constructed two prototype half-barrels (four will be needed for the final phase 1 pixel system) including both detector and supply tube parts as shown in Fig. 11.14. The prototypes are currently tested at CERN. The mechanical construction of the cooling system is very challenging, in particular the brazing of thin, stainless steel tubes in dense and inclined positions. We are still performing stress tests at the workshop here at the University of Zurich and investigate aging effects to confirm the reliability and the longterm stability of the brazing process in view of final construction.

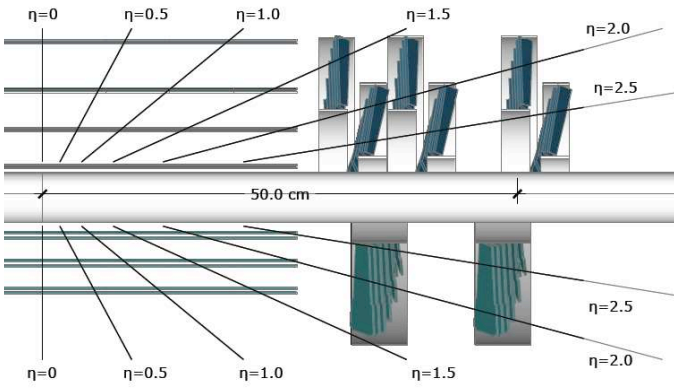

FIG. 11.13 – Schematic of barrel pixel upgrade. Bottom half represents current 3-layer BPIX system, top half shows upgraded 4-layer system in which the innermost detector plane is located within 3 cm of the beam axis.

In addition to the commitment in the construction of the mechanical support system of the CMS pixel phase 1 upgrade, our group is also responsible for the integration of the supply tube readout electronics and the testing of the complete system. The barrel pixel supply tube supports ten types of electronics boards which communicate with the pixel modules to handle control signals, DC-DC power conversion and power distribution, data readout, electrical to optical signal conversions, communication with the DAQ, as well as the cooling loop structure.

In order to test the performance of the complete pixel system we are installing a full CMS-pixel DAQ system at the University of Zurich, commission it and write the necessary software. The system makes use of power supplies, control modules, a DCS system, two readout systems (VME until 2016, μTCA 2017 and after) as well as additional equipment to handle the complex fiber arrangements and to check the fiber connections.

Prototypes of all electronics components have become available during this past year and were integrated together with two pixel detector modules in our system test as shown as shown in Fig. 11.15. Our goal is to gain experience in the operation of the new system and validate the individual components in view of the final production. Testing has started, but considerable work is still needed over the coming months to operate together all the detector parts and in the development of sophisticated software algorithms for testing, calibration and monitoring of all detector components.

[1] A. Burgmeier and D. Pitzl, CMS-AN-13-356.

[2] CMS collaboration, CERN-LHCC-2012-016 (2012).

FIG. 11.14 – One of the two half-barrel prototypes of the phase 1 pixel upgrade cooling system.

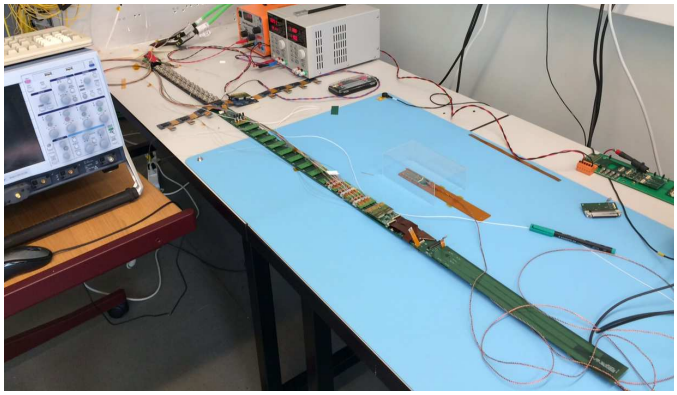

FIG. 11.15 – The CMS pixel phase 1 system test setup at University of Zurich. The test setup includes a detector module connected to the chain of readout electronics that will be hosted on the supply tube.